Article

First Report on the Geologic Occurrence of Natural Na–A Zeolite and Associated Minerals in Cretaceous Mudstones of the Paja Formation of Vélez (Santander), Colombia

Carlos Alberto Ríos-Reyes [1,*] , **German Alfonso Reyes-Mendoza** [2], **José Antonio Henao-Martínez** [3] , **Craig Williams** [4] **and Alan Dyer** [5]

1   Escuela de Geología, Universidad Industrial de Santander, Bucaramanga 680001, Colombia
2   Facultat de Ciències de la Terra, Universitat de Barcelona, 680001 Barcelona, Spain; georeycol@yahoo.es
3   Escuela de Química, Universidad Industrial de Santander, Bucaramanga 680001, Colombia; jahenao@uis.edu.co
4   School of Applied Sciences, University of Wolverhampton, Wolverhampton WV1 1LY, UK; c.williams@wlv.ac.uk
5   Retired Prof Founder Member of the British Zeolite Association, Wolverhampton WV1 1LY, UK; aldilp@aol.com
*   Correspondence: carios@uis.edu.co

Abstract: This study reports for the first time the geologic occurrence of natural zeolite A and associated minerals in mudstones from the Cretaceous Paja Formation in the urban area of the municipality of Vélez (Santander), Colombia. These rocks are mainly composed of quartz, muscovite, pyrophyllite, kaolinite and chlorite group minerals, framboidal and cubic pyrite, as well as marcasite, with minor feldspar, sulphates, and phosphates. Total organic carbon (TOC), total sulfur (TS), and millimeter fragments of algae are high, whereas few centimeters and not biodiverse small ammonite fossils, and other allochemical components are subordinated. Na–A zeolite and associated mineral phases as sodalite occur just beside the interparticle micropores (honeycomb from framboidal, cube molds, and amorphous cavities). It is facilitated by petrophysical properties alterations, due to processes of high diagenesis, temperatures up to 80–100 °C, with weathering contributions, which increase the porosity and permeability, as well as the transmissivity (fluid flow), allowing the geochemistry remobilization and/or recrystallization of pre-existing silica, muscovite, kaolinite minerals group, salts, carbonates, oxides and peroxides. X-ray diffraction analyses reveal the mineral composition of the mudstones and scanning electron micrographs show the typical cubic morphology of Na–A zeolite of approximately 0.45 mμ in particle size. Our data show that the sequence of the transformation of phases is: Poorly crystalline aluminosilicate → sodalite → Na–A zeolite. A literature review shows that this is an unusual example of the occurrence of natural zeolites in sedimentary marine rocks recognized around the world.

Keywords: natural zeolite A; mineralogy; mudstones; crystal; sedimentary environment

1. Introduction

The Swedish mineralogist Axel Fredrick Cronstedt discovered in 1756 the stilbite in allusion to their visibly lost water when heated and named the group of zeolites (from the Greek words "zeo" meaning "to boil" and "lithos" meaning "stone"). Nearly 250 years have passed since this discovery, and geologists traditionally have considered that natural zeolites are formed during aqueous fluids reaction with rocks in a variety of geological environments [1–6]. Several occurrences of natural zeolites have been reported worldwide as accessory minerals in the vugs and cavities of basalts and other basic igneous rocks, as major constituents of many bedded pyroclastic deposits and are thought to be among the most widespread and abundant authigenic silicate minerals in sedimentary rocks [1,4]. Most natural zeolites form during diagenetic processes in sedimentary rocks [7–9]. Zeolites

occurring in volcanic lava flow cavities are formed either during lava pile burial metamorphism [10–12], continental basalts' hydrothermal alteration [11,13] or diagenesis in areas of high heat flow caused by active geothermal systems [12,14,15]. Zeolites, as products of hydrothermal crystallization, are generally known from active volcanic rock-associated geothermal systems. Very little work has been published on zeolite occurrences related to late stage pegmatite crystallization [16] in hydrothermal ore veins [17] as alteration products along fault planes [18] and in hydrothermal fractures and veins in granites and gneisses [19]. Zeolites are crystalline, microporous, hydrated aluminosilicates of alkaline or alkaline earth metals. The framework consists of $[SiO_4]^{4-}$ and $[AlO_4]^{5-}$ tetrahedra, which corner-share to form open structures; such tetrahedra are linked to each other by sharing all of the oxygen to form interconnected cages and channels containing mobile water molecules and alkali and/or alkaline earth cations [2,3,20,21]. Zeolites have been widely used as catalysts, adsorbents, and ion exchangers in many technical applications due to their exceptional properties such as extremely high adsorption capacity, catalyzing action, thermal stability, and resistance in different chemical environments [2,22–31]. Zeolites have been extensively used in various technological applications, which include oil refining processes such as catalytic cracking [32,33], as molecular sieves for separating and sorting molecules [34], as adsorbents for water, soil, and air purification [27,35–39] for removing radioactive contaminants [40], for harvesting waste heat and solar heat energy [41], as detergents [42], as antibacterial [43], as drug delivery for oral and topical administration [44,45] or feeding additives for farm animals [46]. They have become worthy of being called the mineral of the future of several countries around the world that have made significant progress in exploring and exploiting this mineral. However, only a few of the natural zeolites in the world are found in sufficient quantities and have the purity required by the industry. The US Geological Survey has reported natural zeolites' worldwide occurrence in the USA, Japan, Korea, Bulgaria, Czechoslovakia, Romania, Hungary, Russia, Croatia, Serbia, South Africa, Italy, Germany, Turkey, and China, the latter having the greatest worldwide production clinoptilolite, mordenite, heulandite, chabazite, phillipsite, and laumontite. At least 60 species of natural zeolites are known to exist, occurring naturally in soils, sediments, and rocks [47], predominantly concentrated in those rocks and soils of volcanic origin. The aim of this study is to report for the first time the geologic occurrence of natural zeolite A and associated minerals in the urban area of Vélez (Santander), Eastern Cordillera, Colombia (Figure 1).

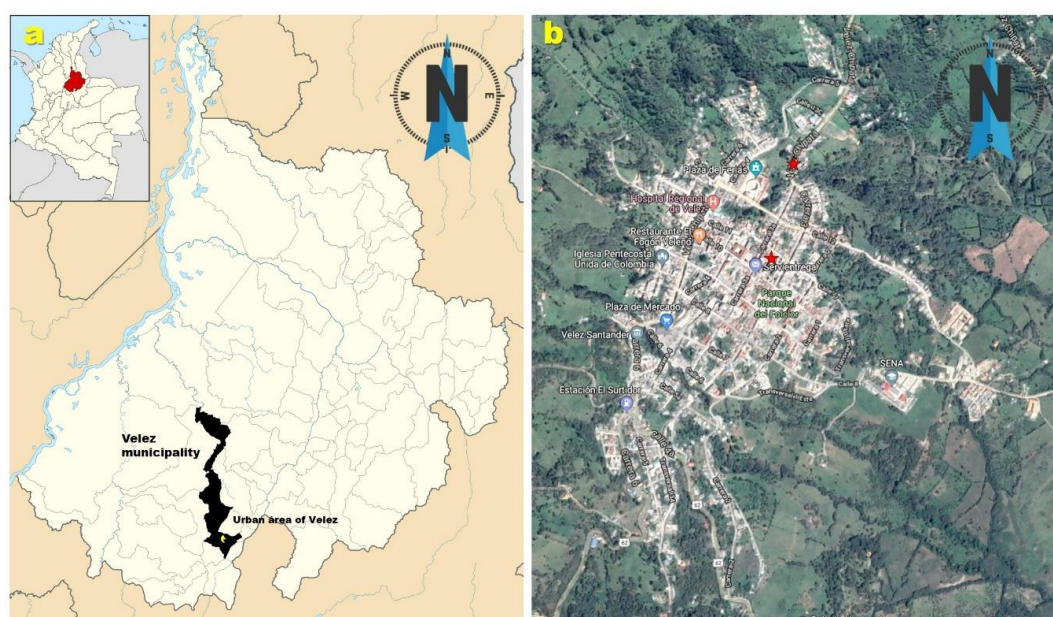**Figure 1.** (**a**) Location of the municipality of Velez (Santander), Colombia, and its urban area. (**b**) Satellite image of the urban area of Vélez, showing the sampling localities indicated by red stars (adapted and modified from Google Maps [48]).

2. Materials and Methods

The investigated samples correspond to mudstones and regoliths, of road cuts and excavations for houses, from the La Paja Formation, in the Eastern Cordillera, over the Northern Andes. A preliminary visual inspection of the samples was performed by conventional petrography (results not shown). More detailed analyses were performed by means of X-ray powder diffraction (XRPD), field emission gun-environmental scanning electron microscopy/energy dispersive X-ray spectroscopy (FEG-ESEM/EDS), and Fourier transform infrared with attenuated total reflection (FTIR-ATR) spectroscopy. The bulk mineralogical composition was determined via XRPD using a BRUKER D8 ADVANCE X-ray diffractometer equipped with operating in Da Vinci geometry and equipped with an X-ray tube (Cu-Kα1 radiation: λ = 1.5406 Å), a one-dimensional LynxEye detector (with aperture angle of 2.93°), a divergent slit of 0.6 mm, two soller axials (primary and secondary) of 2.5°, and a nickel filter. All samples were milled in an agate mortar to a particle size of less than 50 μm and then mounted on a sample holder of polymethylmethacrylate (PMMA) using the filling front technique prior to the XRPD analysis. Data collection was carried out at 40 kV and 30 mA in the 2θ range of 3.5–70°, with a step size of 0.01526° (2θ) and counting time of 1 s/step. Phase identification was performed using the crystallographic database Powder Diffraction File (PDF-2) from the International Centre for Diffraction Data (ICDD) and the Crystallographica Search-Match program. The microstructure and chemical composition were examined using the back-scattered electron (BSE) imaging and EDS analysis on a FEI QUANTA 650 FEG-ESEM, under the following analytical conditions: Magnification = 100–20000×, WD = 9.0–11.0 mm, HV = 20 kV, signal = BSE in ZCONT mode, detector = BSED, EDS Detector EDAX APOLO X with a resolution of 126.1 eV (in. Mn Kα). Structural characterization from the functional groups was performed by FTIR-ATR, using a computer model THERMO SCIENTIFIC IS50, with diamond crystal in the spectral range 400–4000 cm^{-1}.

3. Results

3.1. Field Occurrence

The urban area of Vélez (Santander), Colombia, is sitting on mudstones (Figure 2a,b) of the Paja Formation of the Barremian to Lower Aptian age, which is petrographic and biostratigraphically divided into four segments (Kip1, Kip2, Kip3, and Kip4) and has a large detrital contribution (<40%, primary quartz and muscovite and few microcline), with aluminum-silicates of Na, K, Fe, Ti, Ca, Mg, and P (in crystalline and other amorphous phases = 30%, and biogenic particles (approximately 25%), in an open sea (not of platform), and of low energy level [49]. According to Lazar et al. [50], they can also be classified as ar-fMs-Cs and ca-cMs-Zs shales. Macquaker and Adams [51] considered that they range from sand and silt-bearing clay-rich mudstone to clay-dominated mudstone. Reyes-Mendoza [49] indicated dark gray and carbonaceous mudstones, rather than shales for the absence of fissility, with important microfabric features, such as massive facies dominant, thinly microbial laminae, wavy micro-lamination, not parallel and discontinuous, curled to silty lenticular lamination, massive fossiliferous, locally micro-tempestites, as well as nodules and/or concretions, towards the top grain-growing slightly, beds (sandy facies), and thin layers of fine sandstone. Meanwhile, in the bottom near muddy sequence no evaporitic facies (gypsum) happens. Other abundant minerals are kaolinite and pyrophyllite, iron sulfides (primary framboidal or euxinic pyrite, <5 mμ; autigenic cubic pyrite, and amorphous or anhedral marcasite), organic matter (laminated, amorphous, discrete or in organo-mineralogical aggregates, OMA) with high TOC (>4.64%), sulfur (4.80%), sulphates and inorganic phosphates, amines and aliphatic hydrocarbons. They are not considered calcareous (Ca < 4.30%), with dolomite-ankerite, scarce calcite and some irregular lenses or hollow nodules of several oxides-oxyhydroxides and sodalite, hydrosodalite, as well as crystoballite [49]. Other phyllosilicates are clinocloro, berlinite, chamosite, nacrite (assembly that could indicate a low-grade regional metamorphism or high diagenesis with pyrophyllite, up to 21%), dickite, illite, gibbsite, halloysite, kaolinite, phlogopite, vermi-

culite, phengite and zeolite as products of weathering, the last of them described in detail in this study. Abundant millimetric fragments of phaeophyta and punctually gyrogonites of karophites occur, which indicate a bloom of algae in the superior column of the water. Other allochemicals are ammonites (in molds <5 cm), consolidated intraclasts (<500 μm), few foraminiferous, agglutinated and bilobulates, pyritized radiolarians, calcareous filaments, as well as bone remains in the lower and middle part. Primary intragranular, intergranular, intercrystalline, and low porosity (<5%) was identified compared with secondary porosity, associated with structural discontinuities: Stratification, lamination, jointing, irregular fractures, and probably regional foliation [52]. Reyes-Mendoza [49] evaluated and mapped eight colluviums units (Figure 2c,e) based on their sedimentology, morphological position, and paleosoils of beige-orange colors, as well as thicknesses of 1.5–2.2 m under the old houses of the municipality of Vélez (historical center itself), protected by the hard surfaces of the urban development.

Figure 2. Occurrence of (**a**,**b**) a mudstone outcrop of the Kip3 segment of the Paja Formation along the cutting slope in the San Luis neighborhood, and (**c**–**e**) a regolith of the Kip2 segment of the Paja Formation and excavation in the Las Nieves neighborhood.

3.2. Framework of Zeolite LTA

As shown in Figure 3, zeolite Lynde type A (LTA) displays a three-dimensional framework obtained when periodic building units (PerBUs) (which are built using the sodalite cage (or β-cage) consisting of 24 T atoms (six 4-rings, four 6-rings, three 6-2 units or four 1-4-1 units)), related by pure translations along the cube axes, are linked through double 4-rings (D4Rs) for one cube face. It is made of secondary building units 8 or 4-4 or 6-2 or 6 or 1-4-1 or 4 and composite building units D4R, SOD (or β-cage), and LTA (or α-cage) [53]. The pore diameter is defined by an eight-member oxygen ring and is small at 4.2 Å, which leads into a larger cavity of minimum free diameter 0.41 Å [54]. It contains cages and channels in their negatively charged frameworks due to the substitution of Si^{4+} by Al^{3+} and cations that can enter its porous structure to balance the charge of its structural framework. The general chemical formula of zeolite LTA is $[Na_{12}(Al_{12}Si_{12}O_{48})27H_2O]$, which shows that it has 12 tetrahedra in every cell unit, occupied by 12 Na atoms and 27 H_2O molecules [55], with a cubic unit cell (*a* = 11.9Å), space group Pm-3m [53], and Si/Al ratio of 1 [56].
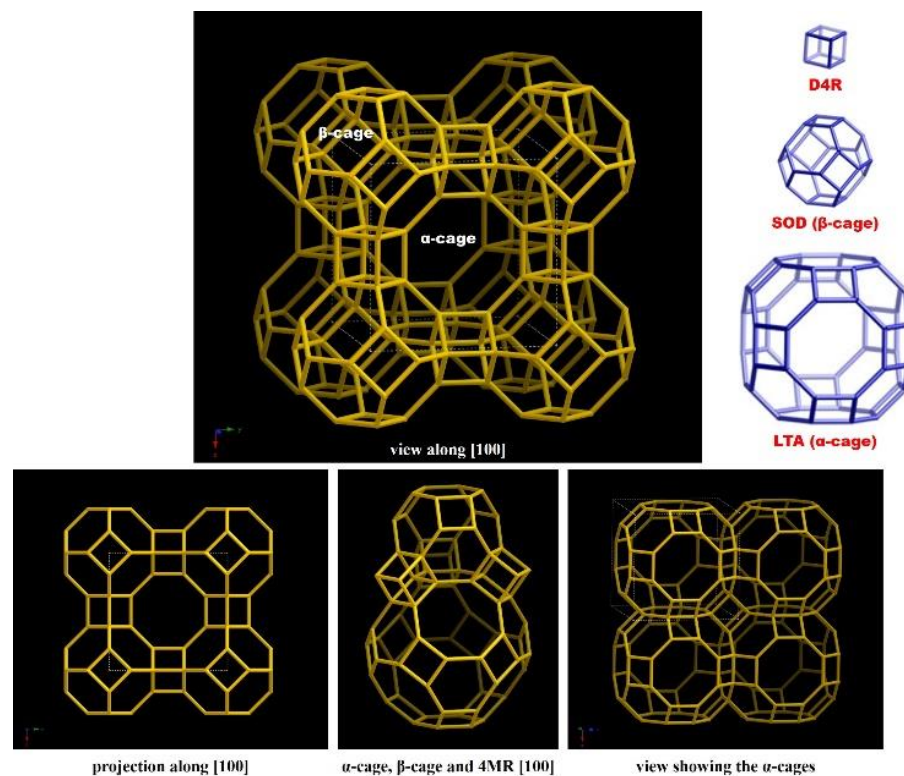

Figure 3. The structural framework of zeolite Lynde type A (LTA), showing its characteristic cages and channels. The vertices mark the positions of the T atoms, the lines symbolize the oxygen bridges between them. Diamond Crystal Structure Software Version 2.1 (structural data published by the International Zeolite Association).

3.3. X-Ray Diffraction

Figure 4 illustrates the characteristic X-ray diffraction pattern of the analyzed mudstone, which reveals high intensity peaks associated with the presence of dickite, illite, and pyrophyllite. Na–A zeolite and sodalite show low intensity peaks. Low intensity peaks correspond to quartz, goethite, and lepidocrocite. Experimental work by Heller-Kallai and Lapides [57] showed that the transformation of kaolinite and metakaolinite with aqueous sodium hydroxide under hydrothermal conditions, with sodalite as the primary product was obtained from kaolinite, whereas the use of metakaolinite promoted the formation of mainly Na–A zeolite, in some cases associated with minor amounts of faujasite. The XRD patterns show the occurrence of a mixture of different mineral phases,

including Na–A zeolite and sodalite: Quartz (12.1–19.1 wt%); muscovite (1.5 wt%); pyrophyllite (4.0–19.6 wt%); lepidocrocite (2.8 wt%); kaolinite (1.0 wt%); dickite (13.2 wt%); illite (7.0–11.1 wt%); goethite (10.1 wt%); titanomagnetite (1.0 wt%); zeolite A (2.5 wt%); zeolite X (0.1–4.1 wt%); zeolite SSZ-35 (8.6 wt%). Crystalline phases (55.4–62.9 wt%); amorphous, etc. (37.1–44.6 wt%).
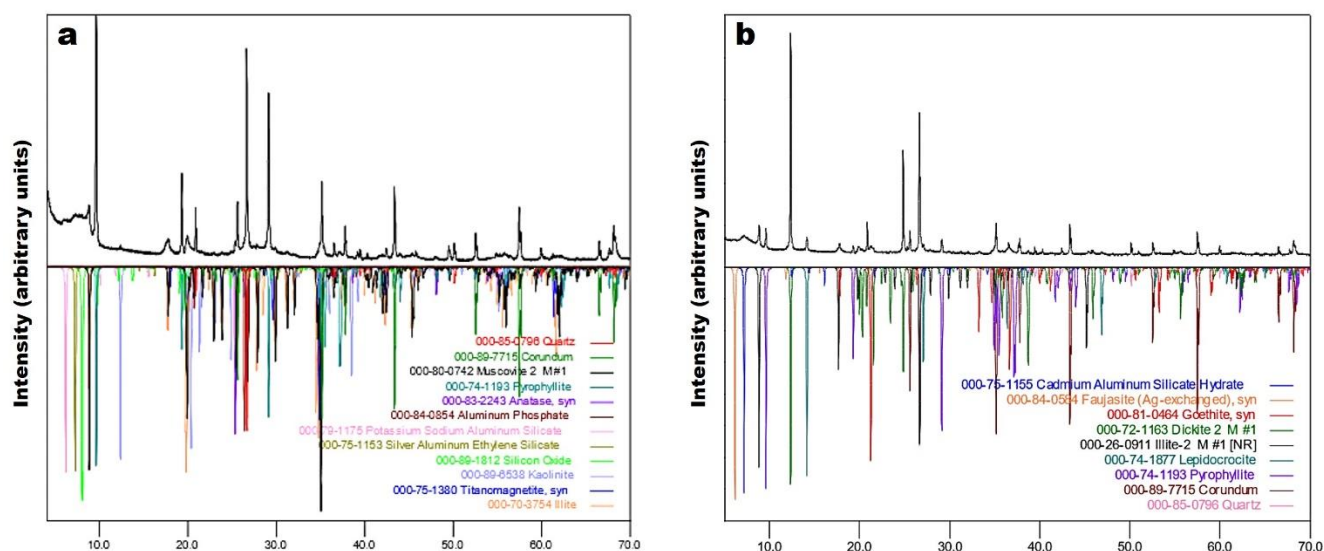

Figure 4. XRD pattern of the analyzed (**a**) mudstone and (**b**) regolith. Qtz: Quartz; Ms: Muscovite; Pyr: Pyrophyllite; Lpd: Lepidocrocite; Kao: Kaolinite; Dck: Dickite; Ill: Illite; Goe: Goethite; TiMag: Titanomagnetite; LTA: Na–A zeolite; FAU: Faujasite; SSZ: Zeolite SSZ-35.

3.4. Scanning Electron Microscopy

SEM micrographs (Figure 5) illustrate the occurrence of the mudstone of the Kip3 segment of the Paja Formation. The morphological features of this rock show randomly interstratified clay minerals with developed sheet structures, bedding planes, and crystal morphology, as well as migration pathways and microporosity (Figure 5a). The bedding planes are broken by rounded and cubic micropores associated to framboidal and cubic pyrite, respectively (Figure 5b). Figure 5c shows the occurrence of aggregates of Na–A zeolite and sodalite. Na–A zeolite displays a typical cubic morphology, whereas sodalite develops aggregates of randomly oriented and intersecting blade-shaped crystals. Ríos et al. [58] described spherical agglomerates of sodalite growing out onto the surface of well-developed cubes of Na–A zeolite displaying fluorite-type interpenetration twinning, which indicates that it is a thermodynamically metastable phase which was successively replaced by a more stable phase as sodalite. Figure 5d,f illustrates the typical appearance of kaolinite occurring as aggregates composed of pseudohexagonal plates, which also constitutes the rock matrix.
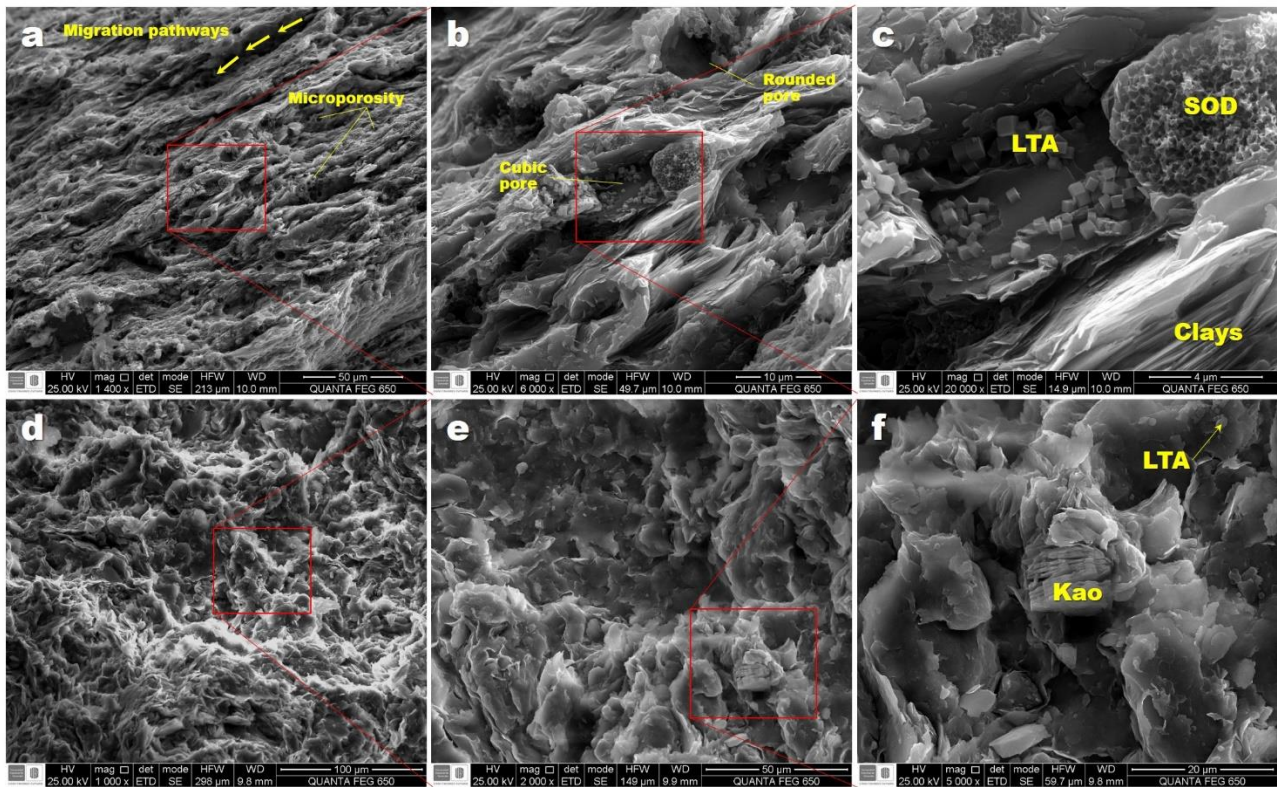
Figure 5. Secondary electron (SE) images of the (**a**) morphological features of the wavy micro-lamination, not parallel and discontinuous, fabric of the analyzed mudstone, (**b**) microporosity, (**c**) aggregates of Na–A zeolite and sodalite and clays, and (**d**–**f**) aggregates of clays of kaolinite-type in the matrix. LTA: Na–A zeolite; SOD: Sodalite; Kao: Kaolinite.

Figure 6 illustrates SE images of the occurrence of aggregates of cubic Na–A zeolite and honeycomb sodalite in the pore space left by the oxidation of cubic and framboidal pyrite (upper part), and the typical EDS spectra of Na–A zeolite and associated mineral phases (lower part). Clay minerals occurring in the matrix of the mudstone reveal the presence of high concentrations of Al (16.51 wt%), Si (29.01 wt%), and O (24.78 wt%). Na–A zeolite shows high concentrations of Al (17.97 wt%), Si (27.14 wt%), and O (9.63 wt%). Sodalite shows high concentrations of Al (17.65 wt%), Si (35.30 wt%), and O (16.38 wt%). The peaks of Fe, Mg, Na, K, S, and Ti (results not shown) represent the contribution of associated mineral phases such as pyrite, Ti-oxides, and feldspars. The peak of Au in the spectra is attributed to the gold coating.

The SE image and EDS spectrum of the analyzed Na–A zeolite are shown in Figure 7. Na–A zeolite displays a typical cubic morphology, which is broken by the presence of aggregates of sodalite, which develops from randomly oriented and intersecting blade-shaped crystals growing at expenses of Na–A zeolite. It shows high concentrations of Al (17.97 wt%), Si (27.14 wt%), and O (9.63 wt%). The peaks of Fe, Mg, Na, K, S, and Ti (results not shown) represent the contribution of associated mineral phases such as pyrite, Ti-oxides, and feldspars. The peak of Au in the spectra is attributed to the gold coating.
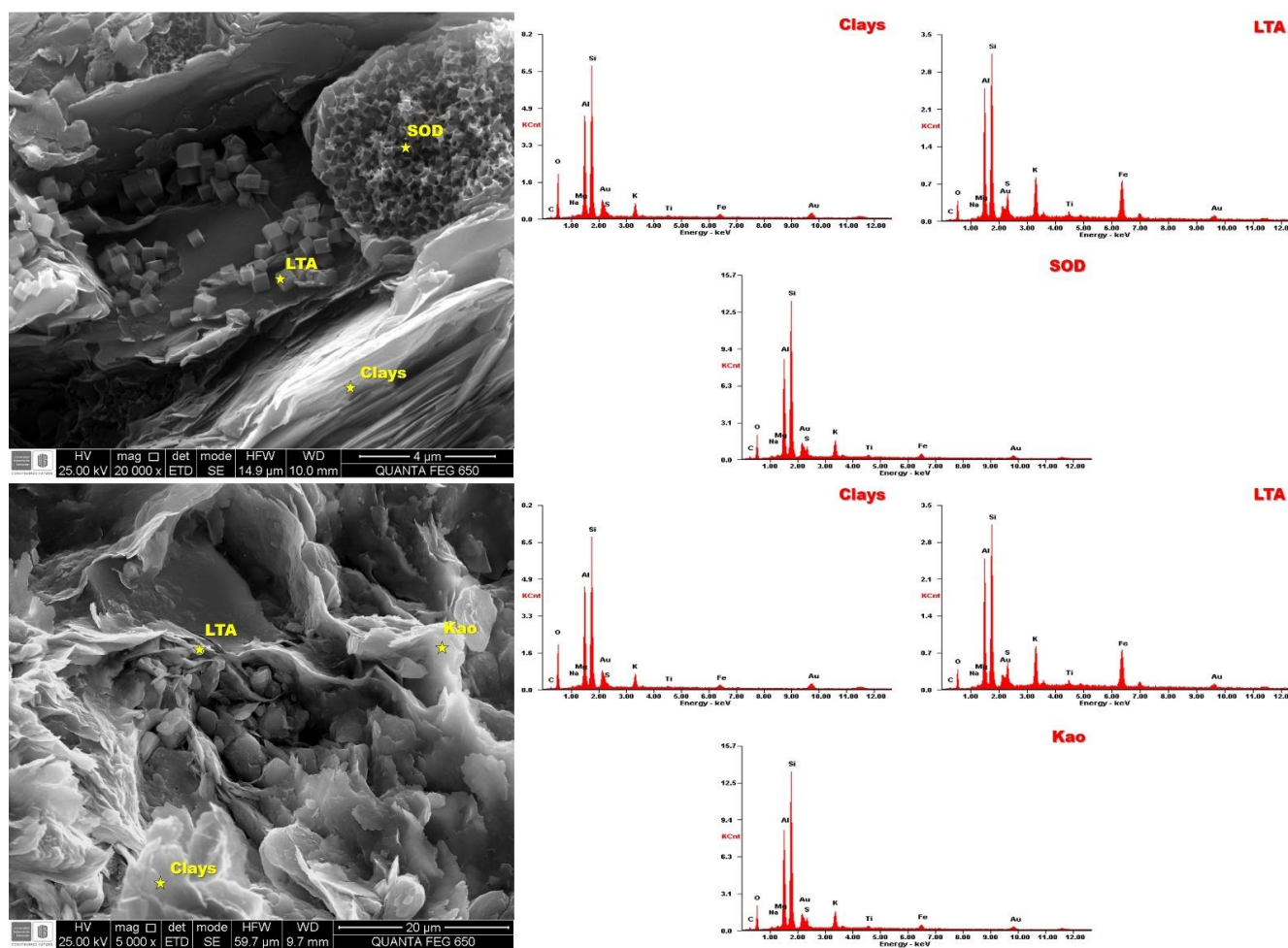
Figure 6. SE images of the analyzed aggregates of Na–A zeolite, sodalite, and clays. LTA: Na–A zeolite; SOD: Sodalite; Kao: Kaolinite.
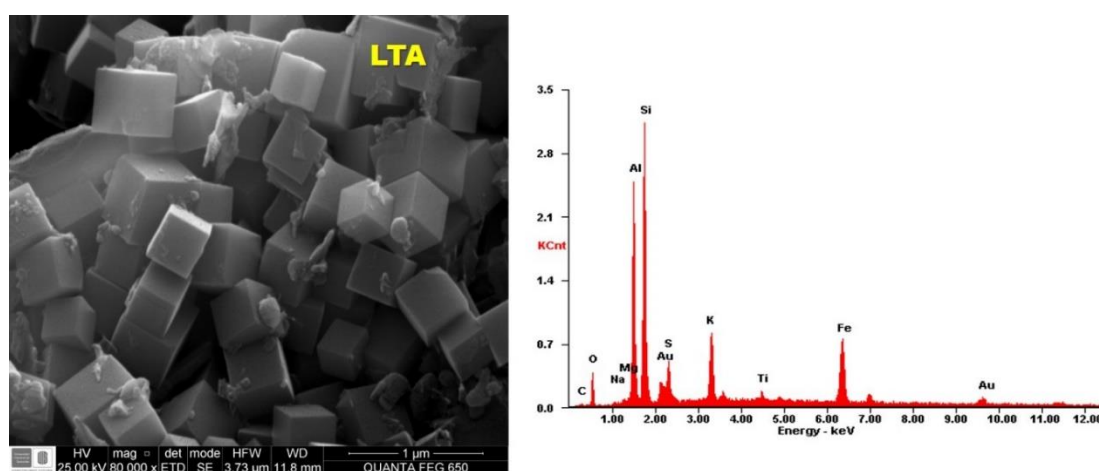

Figure 7. SE image (**left**) and EDS spectrum (**right**) of Na–A zeolite (LTA).

3.5. Fourier Transform Infrared with Attenuated Total Reflection Spectroscopy

FTIR spectra in Figure 8 show the typical vibration bands of the analyzed mudstone and regolith. We recognize the characteristic OH-stretching vibrations of kaolinite at 3698 cm^{-1} (surface OH stretching) and 3620–3629 cm^{-1} (inner OH stretching). How-

ever, the vibration band at 3620 cm^{-1} can also be attributed to gibbsite. The vibration bands at 1621 cm^{-1} (kaolinite), 1630 cm^{-1} (goethite or calcite), 1420–1423 cm^{-1} (calcite or siderite), 979 cm^{-1} (gibbsite), 987 cm^{-1} (chlorite), 929 and 907 cm^{-1} (margarite or kaolinite), 820–822 cm^{-1} (phlogopite or margarite), 792–796 cm^{-1} (quartz or goethite), 746 cm^{-1} (muscovite or dickite), 693 cm^{-1} (quartz, kaolinite, phlogopite or margarite), 687 cm^{-1} (kaolinite), 518 cm^{-1} (phlogopite), 512 cm^{-1} (margarite), 441–443 cm^{-1} (potassium feldspar, chlorite or margarite), 415 cm^{-1} (margarite), 411 cm^{-1} (muscovite), and 401 cm^{-1} (margarite) were also observed. The major structural groups present in zeolites can be detected from their FTIR patterns. The band at 1621–1630 cm^{-1} can be attributed to zeolitic water. However, the region of 1500–400 cm^{-1} is a fingerprint indicating structural features of zeolite frameworks. On the other hand, characteristic bands of zeolitic materials appeared, including the asymmetric Al–O stretch located in the region of 1250–950 cm^{-1} (with the bands at 979 and 987 cm^{-1} assigned to sodalite) and their symmetric Al–O stretch located in the region of 660–770 cm^{-1}. Similar results have been reported by several studies [37,59–63]. There is a well-defined peak at 693 cm^{-1} assigned to symmetric T–O–T vibrations of the sodalite framework in good agreement with the results reported by Flaningen et al. [59]. The peak at 687 cm^{-1} can be attributed to the Na–A zeolite. The bands in the region of 500–650 cm^{-1} are related to the presence of the double rings (D4R and D6R) in the framework structure of sodalite. The bands in the region of 420–500 cm^{-1} are related to internal tetrahedron vibrations of Si–O and Al–O of sodalite. The bands at 441–443 cm^{-1} are related to internal tetrahedron vibrations of Si–O and Al–O of sodalite (T–O–T) bending modes of the sodalite framework. The detailed FTIR assignments for sodalite have been summarized by Barnes et al. [60] and later revised by Zhao et al. [64]. The bands in the region of 400–420 cm^{-1} are related to the pore opening or motion of the tetrahedral rings, which form the pore opening of zeolites [2].
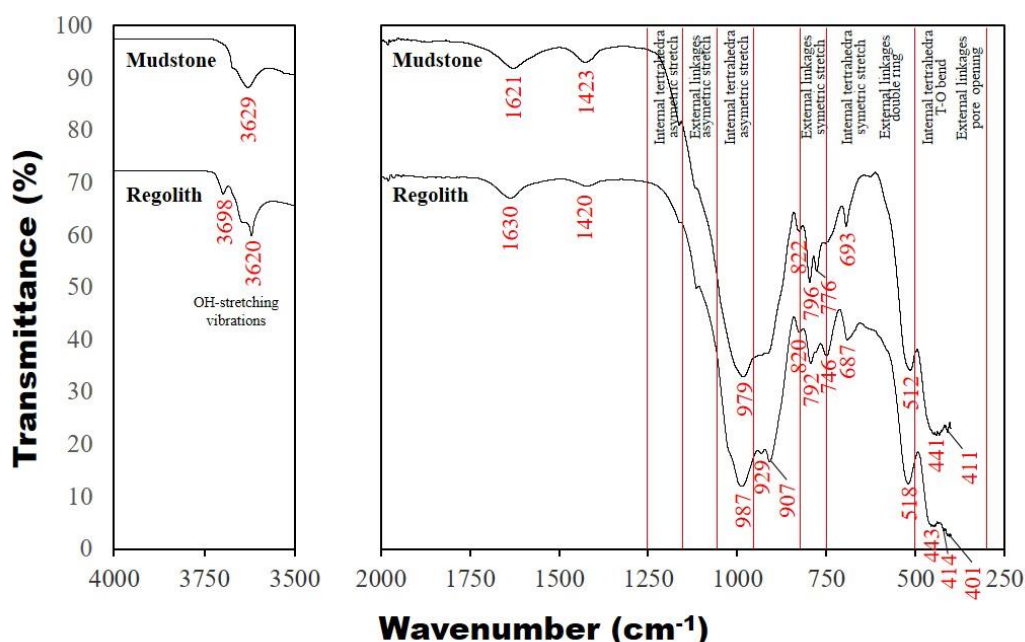

Figure 8. FTIR spectrum of the analyzed mudstone and regolith.

3.6. Discussion on the Mechanism of Formation of the Na–A Zeolite in Mudstone and Regolith

One of the main challenges facing geosciences is to reconstruct the environments in which minerals are formed. Several research groups have performed experimental work to successfully bridge the gap between the general formation mechanisms of crystalline phases and the crystallization of complex structures, such as those of zeolites [21]. We evaluate the geological characteristics of mudstone and regolith systems, taking in con-

sideration not only their mineralogy but also the environmental conditions, which can be strongly affected by several factors, revealing a complex history of chemical reactions in the origin of zeolitic materials. The Cretaceous Paja Formation formed in closed basin environments with low water circulation and small oscillations in the relative sea-level [65,66]. For dissolution of mudstone grains and precipitation of authigenic minerals to occur on the weathered horizon of the La Paja Formation are circulating fluids for the transport of nutrients (ions), geochemical processes, and biogenic activity, which modifies porosity and permeability that will allow fluid migration. According to Passaglia et al. [67], the main factors that control the species and precipitation of diagenetic zeolites are the texture and composition of the host rock, composition of the fluids, and temperature. Na-enriched zeolites, such as the Na–A zeolite, tend to form through the rock-strongly alkaline (pH > 10) fluid interaction which are in a hydrologically closed system [22,67]. The SiO_2 and Al_2O_3 sources for the formation of Na–A zeolite is speculative, taking into account that volcanic glass, the source for many diagenetic zeolites, is not present in La Paja Formation rocks. However, the Na–A zeolite may form where the supply of mobile ions nearly equals the supply of Si and Al [68]. The chemical weathering of mudstones can be characterized by a sequence of chemical reactions between percolating groundwater and rock-forming minerals, with pyrite probably playing a very important role. Pyrite and other sulphides were affected by oxidation (by oxygen coming from the ground surface) to form sulfuric acid (H_2SO_4), sulfate minerals (e.g., gypsum), and several iron oxides such as goethite and hematite, developing an oxidation zone. Framboidal (raspberry-like) pyrite is found representing the most problematic form in terms of the effects of pyrite oxidation. Taking into account the fact that the oxidation of pyrite is primarily surface controlled, the reactivity of pyrite increases as the grain size decreases and the relative surface area increases [69]. The H_2SO_4, along with atmospheric agents, salts, inorganic and biogenic acids, dissolves rock-forming minerals, developing a dissolved zone. The few carbonates (mainly dolomite), which are buffering minerals (the acidity of the medium was neutralized) were dissolved in rhombohedral molds. However, it is probably that this did not occur in the analyzed samples where framboidal (raspberry-like) pyrite suffered oxidation. Taking into account the fact that alkaline pH tends to inhibit pyrite dissolution by blocking the access of the oxidizing agent (O_2) to pyrite surfaces [70,71]. Nanobacteria were observed, which possibly degrade amino acids and produce sulphites that nourish plants. Therefore, the weathering is strongly conditioned by physical, chemical, and biological processes. Consequently, the acidity of the system is neutralized and other elements silicon, aluminum, sodium, potassium, calcium, iron, magnesium, titanium, and phosphorus are released, which enter into the solution or precipitate within the mudstone or regolith (originally composed of clay minerals (about 50–60 wt%) and other minerals, especially quartz and carbonates), originating secondary minerals, such as new clays, zeolites, iron oxides, and hydroxides, etc. The clay minerals in mudstone are largely kaolinite and illite, which are excellent indicators of the environment due to their sensitivity to slight changes in the composition, temperature, and pH of their surroundings [72]. Different clay minerals have been used as starting materials with an appropriate SiO_2/Al_2O_3 ratio for studying the formation of zeolites at the laboratory scale [2–64,73–90]. However, kaolinite has been of interest in several studies. It varies in terms of the structural make up from one deposit to another, consists of dioctahedral 1:1 layer structures with a composition of $Al_2Si_2O_5[OH]_4$. This variation affects the ordering of the kaolinite structure and their subsequent chemical reactivity. Previous studies reveal that the improvement of the properties of the kaolinite by chemical methods is difficult due to its low reactivity, taking into account the fact that it is not significantly affected under acid or alkaline conditions [63,91–93]. Therefore, kaolinite is usually used after calcination at temperatures between 550–950 °C [37,91,92,94–96] to obtain a more reactive phase (metakaolinite). However, this clay mineral is not stable under highly alkaline conditions and different zeolitic materials can form. Several authors have reported the synthesis of kaolinite-based zeolites, including LTA [96–98], FAU [85,91,96,98,99], GIS [96,100], CAN [64,101], SOD [64,101,102], and JBW [37,103,104].

According to Zhao et al. [64], there are two major chemical processes involved in the reaction between kaolinite and alkaline solutions: Dissolution of kaolinite, releasing Si and Al, followed by the formation of zeolitic materials. In this study, we suggest that the Na–A zeolite clearly formed by precipitation from relatively low temperature fluids in pores of the analyzed samples, which is supported by the experimental work performed by Ríos [37], who obtained the Na–A zeolite along with sodalite and cancrinite under hydrothermal alkaline conditions at 100 °C during a period of reaction time of 6–120 h. It is seen that a higher alkali concentration during the synthesis process leads to a faster dissolution of the original kaolinite, accompanied by more crystalline zeolitic materials. The Na and Mg-enriched geochemistry of the analyzed mudstone and regolith provides additional evidence for alteration, reflecting the low temperature hydrothermal growth of zeolitic materials, which, therefore, are not related to the original sedimentary mineralogy. The genesis of sodic zeolites, such as the Na–A zeolite along with sodalite and cancrinite, was affected by parameters as the reaction temperature and time between the starting materials (mudstone or regolith) and low temperature fluids, the alkalinity (alkaline conditions or high Na content) of the fluids, and the very high Na/K ratio and the necessary SiO_2/Al_2O_3 ratio of the starting materials. Ríos and co-workers [37,58,63,105–109] performed the experimental work in order to simulate the geological conditions and chemical reactions expected during the formation of zeolites. The results of these studies reveal the hydrothermal transformation of kaolinite, with the production of several zeotypes, including sodalite, cancrinite, and Na–A zeolites in agreement with the previous studies. However, Ríos et al. [58] considered that sodalite and cancrinite represent a metastable phase via the Na–A zeolite forming reaction. In the case of a mudstone or regolith system as that reported in the present study, we consider that the chemistry of evolution of the Na–A zeolite was affected by several factors. The reaction history of the formation of the Na–A zeolite reported in this study can be summarized by the following stages: (1) Dissolution of aluminosilicate minerals (clays) in the mudstone or regolith releasing SiO_2 and Al_2O_3, (2) formation of intermediate metastable phases (sodalite), (3) occurrence of simultaneous reactions of precipitation and dissolution of a gel phase, nucleation, and growth of Na–A zeolite that reached chemical equilibrium. The Na–A zeolite is typically crystallized from amorphous aluminosilicate precursors in aqueous in the presence of alkali metals. A simple scheme of the crystallization of an amorphous aluminosilicate hydrogel to the Na–A zeolite is given in Figure 9. At the beginning, a dissolution of the aluminosilicate minerals (clays) in the mudstone or regolith occurred, releasing SiO_2 and Al_2O_3, with the production of an amorphous gel characterized by the presence of small olygomers. A dissolution process promotes the formation of the nutrients (ionic species), which then are transported to the nucleation sites, indicating that the ionic species are not static, since they necessarily need to move (transportation) to the nucleation sites. A nucleation process produced an equilibrated gel. During nucleation, the hydrogel composition and structure are significantly affected by thermodynamic and kinetic parameters. A polymerization of SiO_4 tetrahedra proceeds, which is represented by TO_4 primary tetrahedral building units that have been joined, revealing how they link together to form larger structures. A polymerization is the process that forms the Na–A zeolite precursors, which contains tetrahedral of Si and Al randomly distributed along the polymeric chains which are cross-linked to provide cavities large enough to accommodate the charge balancing alkali ions. During crystal growth, the TO_4 units were linked, with the formation of 4-ring and 6-ring, composed by 4 and 6 tetrahedral atoms, respectively, to create a large structure (secondary building unit) such as the SOD β-cage. The crystallization of Na–A zeolite occurred by linking the same secondary building units together. A phase transformation occurred as represented by the sequence of reaction: Poorly crystalline aluminosilicate → sodalite → Na–A zeolite.
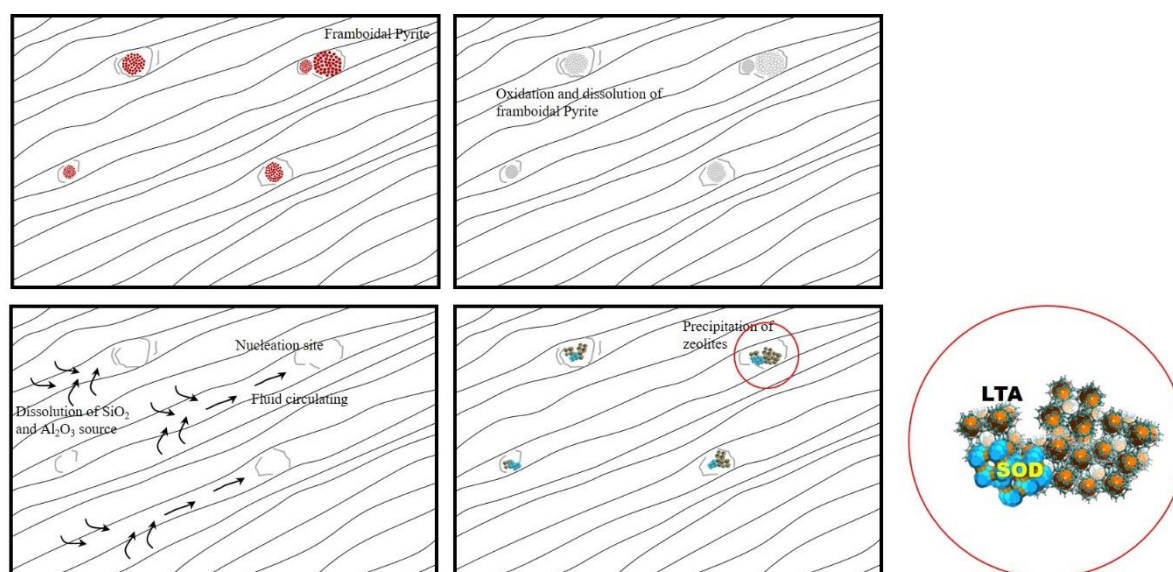
Figure 9. Sketch showing the reconstructed sequence of mineral reactions taking place in the studied mudstone and regolith.

4. Conclusions

In this study, an unusual example of the occurrence of natural zeolites in sedimentary marine rocks was recognized. Na–A zeolite and sodalite occur in mudstones and regoliths of the weathering zone of the Cretaceous La Paja Formation, Vélez (Santander), Colombia.

These rocks consist of quartz, muscovite, abundant pyrophyllite, kaolinite, and chlorite group minerals, pyrite, marcasite, minor feldspar, sulphates, and phosphates, with a high content of TOC, TS, and algae, as well as subordinated ammonite fossils and other allochemical components. High diagenesis (temperatures up to 80–100 °C), weathering, and fluid flow allowed the geochemistry remobilization and/or recrystallization of pre-existing mineral phases.

Our model suggests that the genesis of sodic zeolites, such as Na–A zeolite and sodalite, was affected by parameters as the reaction temperature and time between the starting materials (mudstone or regolith) and low temperature fluids, the alkalinity (alkaline conditions or high Na content) of the fluids, as well as the very high Na/K ratio and the necessary SiO_2/Al_2O_3 ratio of the starting materials. With time, the nucleation and growth process of zeolitic phases involved the dissolution of early metastable phases (Na–A zeolite) and the crystallization of sodalite separated in the same media. However, additional work is necessary to determine their environmental conditions of formation.

Author Contributions: Conceptualization, validation, writing—review and editing, visualization, supervision, funding acquisition, C.A.R.-R.; conceptualization, formal analysis, investigation, methodology, writing—original draft, visualization, project administration, funding acquisition, G.A.R.-M.; conceptualization, validation, investigation, writing—review and editing, supervision, funding acquisition, J.A.H.-M.; conceptualization, validation, investigation, writing—review and editing, supervision, C.W.; conceptualization, validation, investigation, writing—review and editing, supervision, A.D. All authors have read and agreed to the published version of the manuscript.

Institutional Review Board Statement: Not applicable.

Informed Consent Statement: Not applicable.

Data Availability Statement: All data are included in the manuscript.

Conflicts of Interest: The authors declare no conflict of interest.

References

1. Mumpton, F.A. First reported Occurrence of Zeolites in Sedimentary Rocks of Mexico. *Am. Mineral.* **1973**, *58*, 287–290.
2. Breck, D.W. *Zeolite Molecular Sieves: Structure, Chemistry and Use*; John Wiley: New York, NY, USA, 1974; 313p.
3. Gottardi, G.; Galli, E. *Natural Zeolites*; Springer: Berlin/Heidelberg, Germany, 1985; 409p.
4. Ming, D.W.; Mumpton, F.A. Zeolites in soils. In *Minerals in Soil Environments*; Dixon, J.B., Weed, S.B., Eds.; Soil Science Society of America: Madison, WI, USA, 1989; pp. 873–911.
5. Tsitsishvili, G.; Skhirtladze, N.; Andronikashvili, T.; Tsitsishvili, V.; Dolidze, A. Natural zeolites of Georgia: Occurrences, properties, and application. *Prep. Catal. V Sci. Bases Prep. Heterog. Catal. Proc. Fifth Int. Symp.* **1999**, *125*, 715–722. [CrossRef]
6. Weisenberger, T. Zeolites in fissures of crystalline basement rocks. Ph.D. Thesis, Universität Freiburg, Freiburg, Germany, 2009. Unpublished.
7. Boles, J.R.; Coombs, D.S. Zeolite facies alteration of sandstones in the Southland Syncline, New Zealand. *Am. J. Sci.* **1977**, *277*, 982–1012. [CrossRef]
8. Hay, R.L.; Sheppard, R.A. Occurrence of Zeolites in Sedimentary Rocks: An Overview. *Rev. Miner. Geochem.* **2001**, *45*, 217–234. [CrossRef]
9. Langella, A.; Cappelletti, P.; Gennaro, R.D. Zeolites in Closed Hydrologic Systems. *Rev. Miner. Geochem.* **2001**, *45*, 235–260. [CrossRef]
10. Neuhoff, P.S.; Fridriksson, T.; Arnórsson, S. Porosity evolution and mineral paragenesis during low-grade metamorphism of basaltic lavas at Teigarhorn, Eastern Iceland. *Am. J. Sci.* **1999**, *299*, 467–501. [CrossRef]
11. Ballance, P.F.; Waiters, W.A. Hydrothermal alteration, contact metamorphism, and authigenesis in Ferrar Supergroup and Beacon Supergroup rocks, Carapace Nunatak, Allan Hills, and Coombs Hills, Victoria Land, Antarctica. *New Zealand J. Geol. Geophys.* **2002**, *45*, 71–84. [CrossRef]
12. Weisenberger, T.; Selbekk, R.S. Multi-stage zeolite facies mineralization in the Hvalfjördur area, Iceland. *Acta Diabetol.* **2008**, *98*, 985–999. [CrossRef]
13. Walker, G.P.L. Zeolite Zones and Dike Distribution in Relation to the Structure of the Basalts of Eastern Iceland. *J. Geol.* **1960**, *68*, 515–528. [CrossRef]
14. Lagat, J. Hydrothermal alteration mineraology in geotermal fields with case examples from Olkaria Domes Getothermal Field, Kenya. In Proceedings of the Short Course IV on Exploration for Geothermal Resources, organized by UNU-GTP, KenGen and GDC, Lake Naivasha, Kenya, 1–22 November 2009.
15. Kralj, P.; Rychagov, S.; Kralj, P. Zeolites in volcanic-igneous hydrothermal systems: A case study of Pauzhetka geothermal field (Kamchatka) and Oligocene Smrekovec volcanic complex (Slovenia). *Environ. Earth Sci.* **2010**, *59*, 951–956. [CrossRef]
16. Orlandi, P.; Scortecci, P.B. Minerals of the Elba pegmatites. *Mineral. Rec.* **1985**, *16*, 353–364.
17. Deer, W.A.; Howie, R.A.; Wise, W.S.; Zussman, J. *An Introduction to Rock-Forming Minerals*; The Geological Society: London, UK, 2004; 696p.
18. Vincent, M.W.; Ehlig, P.L. Laumontite mineralization in rocks exposed north of San Andreas Fault at Cajon Pass, southern California. *Geophys. Res. Lett.* **1988**, *15*, 977–980. [CrossRef]
19. Weisenberger, T.; Bucher, K. Zeolites in fissures of granites and gneisses of the Central Alps. *J. Metamorph. Geol.* **2010**, *28*, 825–847. [CrossRef]
20. Barrer, R.M. *Hydrothermal Chemistry of Zeolites*; Academic Press: New York, NY, USA, 1982; 360p.
21. Szostak, R. *Molecular Sieves*; Springer: Berlin/Heidelberg, Germany, 1989; p. 359.
22. Booker, N.A.; Cooney, E.L.; Priestley, A.J. Ammonia removal from sewage using natural Australian zeolite. *Water Sci. Technol.* **1996**, *34*, 17–24. [CrossRef]
23. Dixit, L.; Prasada, T.S.R. New approach to acid catalysis and hydrocarbon—Zeolite interactions. *Stud. Surf. Sci. Catal.* **1998**, *113*, 313–319.

24. Loiola, A.; Andrade, J.; Sasaki, J.; da Silva, L. Structural analysis of zeolite NaA synthesized by a cost-effective hydrothermal method using kaolin and its use as water softener. *J. Colloid Interface Sci.* **2012**, *367*, 34–39. [CrossRef]

25. Nuić, I.; Trgo, M.; Medvidović, N.V. The application of the packed bed reactor theory to Pb and Zn uptake from the binary solution onto the fixed bed of natural zeolite. *Chem. Eng. J.* **2016**, *295*, 347–357. [CrossRef]

26. Liu, G.-H.; Wang, Y.; Zhang, Y.; Xu, X.; Qi, L.; Wang, H. Modification of natural zeolite and its application to advanced recovery of organic matter from an ultra-short-SRT activated sludge process effluent. *Sci. Total. Environ.* **2019**, *652*, 1366–1374. [CrossRef]

27. Pinto, G.C.; Ríos, C.A.; Vargas, L.Y. Comparative study on the use of a natural and modified Ecuadorian zeolites of the Cayo Formation on the remediation of an oil-polluted soil. *Ctf–Cienc. Tecnol. Y Futuro* **2019**, *9*, 93–104. [CrossRef]

28. Tran, Y.T.; Lee, J.; Kumar, P.; Kim, K.-H.; Lee, S.S. Natural zeolite and its application in concrete composite production. *Compos. Part. B Eng.* **2019**, *165*, 354–364. [CrossRef]

29. Vargas, A.M.; Cipagauta, C.C.; Molina, D.R.; Ríos, C.A. A comparative study on diclofenac sodium release from surfactant-modified natural zeolites as a pharmaceutical excipient. *Mater. Chem. Phys.* **2020**, *256*, 123644. [CrossRef]

30. Alabbad, E.A. Efficacy assessment of natural zeolite containing wastewater on the adsorption behaviour of Direct Yellow 50 from; equilibrium, kinetics and thermodynamic studies. *Arab. J. Chem.* **2021**, *14*, 103041. [CrossRef]

31. Rey, V.; Ríos, C.; Vargas, L.; Valente, T. Use of natural zeolite-rich tuff and siliceous sand for mine water treatment from abandoned gold mine tailings. *J. Geochem. Explor.* **2021**, *220*, 106660. [CrossRef]

32. Vogt, E.T.C.; Weckhuysen, B.M. Fluid catalytic cracking: Recent developments on the grand old lady of zeolite catalysis. *Chem. Soc. Rev.* **2015**, *44*, 7342–7370. [CrossRef]

33. Suganuma, S.; Katada, N. Innovation of catalytic technology for upgrading of crude oil in petroleum refinery. *Fuel Process. Technol.* **2020**, *208*, 106518. [CrossRef]

34. Cheng, X.-W.; Wang, J.; Huang, Q.; Long, Y.-C. Modified natural STI zeolite–A potentially useful molecular sieve. *Pharmacogenetics* **2007**, *170*, 2080–2085. [CrossRef]

35. Pitcher, S.; Slade, R.; Ward, N. Heavy metal removal from motorway stormwater using zeolites. *Sci. Total. Environ.* **2004**, *334*, 161–166. [CrossRef] [PubMed]

36. Santos, S.; Machado, R.; Correia, M.J.N.; Carvalho, J.R. Treatment of acid mining waters. *Miner. Eng.* **2004**, *17*, 225–232. [CrossRef]

37. Ríos, C.A. Synthesis of Zeolites from Geological Materials and Industrial Wastes for Potential Application in Environmental Problems. Ph.D. Thesis, University of Wolverhampton, Wolverhampton, UK, 2008.

38. Wang, S.; Peng, Y. Natural zeolites as effective adsorbents in water and wastewater treatment. *Chem. Eng. J.* **2010**, *156*, 11–24. [CrossRef]

39. Yang, Y.; Xu, W.; Zhang, F.; Low, Z.-X.; Zhong, Z.; Xing, W. Preparation of highly stable porous SiC membrane supports with enhanced air purification performance by recycling NaA zeolite residue. *J. Membr. Sci.* **2017**, *541*, 500–509. [CrossRef]

40. Marinin, D.V.; Brown, G.N. Studies of sorbent/ion-exchange materials for the removal of radioactive strontium from liquid radioactive waste and high hardness groundwaters. *Waste Manag.* **2000**, *20*, 545–553. [CrossRef]

41. Fujii, S.; Horie, N.; Nakaibayashi, K.; Kanematsu, Y.; Kikuchi, Y.; Nakagaki, T. Design of zeolite boiler in thermochemical energy storage and transport system utilizing unused heat from sugar mill. *Appl. Energy* **2019**, *238*, 561–571. [CrossRef]

42. Cardoso, A.M.; Horn, M.B.; Ferret, L.S.; Azevedo, C.M.; Pires, M. Integrated synthesis of zeolites 4A and Na–P1 using coal fly ash for application in the formulation of detergents and swine wastewater treatment. *J. Hazard. Mater.* **2015**, *287*, 69–77. [CrossRef]

43. Hrenovic, J.; Milenkovic, J.; Ivankovic, T.; Rajic, N. Antibacterial activity of heavy metal-loaded natural zeolite. *J. Hazard. Mater.* **2012**, *201–202*, 260–264. [CrossRef]

44. Faras, T.; Ruiz-Salvador, A.R.; Rivera, A. Interaction studies between drugs and a purified natural clinoptilolite. *Microporous Mesoporous Mater.* **2003**, *61*, 117–125. [CrossRef]

45. Cerri, G.; Farina, M.; Brundu, A.; Daković, A.; Giunchedi, P.; Gavini, E.; Rassu, G. Natural zeolites for pharmaceutical formulations: Preparation and evaluation of a clinoptilolite-based material. *Microporous Mesoporous Mater.* **2016**, *223*, 58–67. [CrossRef]

46. Papaioannou, D.; Katsoulos, P.; Panousis, N.; Karatzias, H. The role of natural and synthetic zeolites as feed additives on the prevention and/or the treatment of certain farm animal diseases: A review. *Microporous Mesoporous Mater.* **2005**, *84*, 161–170. [CrossRef]

47. Rouquerol, J.; Avnir, D.; Fairbridge, C.W.; Everett, D.H.; Haynes, J.M.; Pernicone, N.; Ramsay, J.D.F.; Sing, K.S.W.; Unger, K.K. Recommendations for the characterization of porous solids (Technical Report). *Pure Appl. Chem.* **1994**, *66*, 1739–1758. [CrossRef]

48. Google Maps. 2018. Available online: https://www.google.com/maps/?hl=es (accessed on 31 October 2018).

49. Reyes-Mendoza, G.A. Evaluación detallada e impacto de rocas lodosas meteorizadas. El caso de Vélez (Santander, Colombia). In *Póster y Resumen, en Memorias de la XIII Semana Técnica de Geología, Ingeniería Geológica y Geociencias*; Universidad de Caldas: Manizales, Colombia, 2018; 3p.

50. Lazar, O.R.; Bohacs, K.M.; Macquaker, J.H.S.; Schieber, J.; Demko, T.M. Capturing Key Attributes of Fine-Grained Sedimentary Rocks in Outcrops, Cores, and Thin Sections: Nomenclature and Description Guidelines. *J. Sediment. Res.* **2015**, *85*, 230–246. [CrossRef]

51. Macquaker, J.H.; Adams, A. Maximizing Information from Fine-Grained Sedimentary Rocks: An Inclusive Nomenclature for Mudstones. *J. Sediment. Res.* **2003**, *73*, 735–744. [CrossRef]

52. Reyes-Mendoza, G.A. *Las Rocas Lodosas de Vélez: De la Meteorización a Los Deslizamientos*; Ponencia oral. Fest Station—UIS Inteligente. Seminario U18 Fest—Ideas para transformar El Mundo; Universidad Industrial de Santander: Bucaramanga, Colombia, 23 September 2019.

53. Baerlocher, C.; McCusker, L. Database of Zeolite Structures. 2020. Available online: http://www.iza-structure.org/databases/ (accessed on 15 April 2020).

54. Schüring, A.; Auerbach, S.M.; Fritzsche, S.; Haberlandt, R. On entropic barriers for diffusion in zeolites: A molecular dynamics study. *J. Chem. Phys.* **2002**, *116*, 10890–10894. [CrossRef]

55. García-Soto, A.R.; Rodríguez-Niño, G.; Trujillo, C.A. Zeolite LTA synthesis: Optimising synthesis conditions by using the modified sequential simplex method Síntesis de Zeolita LTA: Optimización de las condiciones de síntesis, usando el método simplex secuencial modificado. *Ing. E Investig.* **2013**, *33*, 22–27.

56. García, A.L.; López, C.M.; Garcia, L.V.; De Goldwasser, M.R.; Casanova, J.D.C. Improvements in the synthesis of zeolites with low Si/Al ratio from Venezuelan sodium silicate for an environmentally friendly process. *Ing. E Investig.* **2016**, *36*, 62–69. [CrossRef]

57. Heller-Kallai, L.; Lapides, I. Reactions of kaolinites and metakaolinites with NaOH—comparison of different samples (Part 1). *Appl. Clay Sci.* **2007**, *35*, 99–107. [CrossRef]

58. Ríos, C.A.; Williams, C.D.; Fullen, M.A. Nucleation and growth history of zeolite LTA as-synthesized from kaolinite by two different methods. *Appl. Clay Sci.* **2009**, *42*, 446–454. [CrossRef]

59. Flaningen, E.M.; Khatami, H.A.; Szymanski, H.A. Infrared Structural Studies of Zeolite Frameworks. In *Molecular Sieve Zeolites, Advances in Chemistry 101*; Flanigen, E.M., Sand, L.B., Eds.; American Chemical Society: Washington, DC, USA, 1971; pp. 201–229.

60. Barnes, M.C.; Addai-Mensah, J.; Gerson, A.R. A methodology for quantifying sodalite and cancrinite phase mixtures and the kinetics of the sodalite to cancrinite phase transformation. *Microporous Mesoporous Mater.* **1999**, *31*, 303–319. [CrossRef]

61. Markovic, S.; Dondur, V.; Dimitrijevic, R. FTIR spectroscopy of framework aluminosilicate structures: Carnegieite and pure sodium nepheline. *J. Mol. Struct.* **2003**, *654*, 223–234. [CrossRef]

62. Byrappa, K.; Suresh-Kumar, B.V. Characterization of Zeolites by Infrared Spectroscopy. *Asian J. Chem.* **2007**, *19*, 4933–4935.

63. Ríos, C.A.; Williams, C.D.; Castellanos, O.M. Nucleation and growth mechanism of sodalite and cancrinite from kaolinite-rich clay under low-temperature hydrothermal conditions. *Mater. Res.* **2013**, *16*, 424–438.

64. Zhao, H.; Deng, Y.; Harsh, J.B.; Flury, M.; Boyle, J.S. Alteration of kaolinite to cancrinite and sodalite by simulated hanford tank waste and its impact on cesium retention. *Clays Clay Miner.* **2004**, *52*, 1–13. [CrossRef]

65. Forero-Onofre, H.; Sarmiento-Rojas, L. *La Facies Evaporítica de la Formación Paja*; Etayo, F., Laverde, F., Eds.; Proyecto Cretácico; Ingeominas: Bogota, Colombia, 1985; Volume 16, pp. 1–16.

66. Rivera, H.A.; Le Roux, J.P.; Sánchez, L.K.; Mariño-Martínez, J.E.; Salazar, C.; Barragán, J.C. Palaeoredox conditions and sequence stratigraphy of the Cretaceous storm-dominated, mixed siliciclastic-carbonate ramp in the Eastern Cordillera Basin (Colombia): Evidence from sedimentary geochemical proxies and facies analysis. *Sediment. Geol.* **2018**, *372*, 1–24. [CrossRef]

67. Passaglia, E.; Vezzalini, G.; Carnevali, R. Diagenetic chabazites and phillipsites in Italy: Crystal chemistry and genesis. *Eur. J. Miner.* **1990**, *2*, 827–840. [CrossRef]

68. Dickinson, W.W.; Grapes, R.H. Authigenic chabazite and implications for weathering in Sirius Group Diamictite, Table Mountain, Dry Valleys, Antarctica. *J. Seidmentary Res.* **1997**, *67*, 815–820.

69. Cripps, J.C.; Taylor, R.K. The engineering properties of mudrocks. *Q. J. Eng. Geol. Hydrogeol.* **1981**, *14*, 325–346. [CrossRef]

70. Nicholson, V.R.; Gillham, W.R.; Reardon, J.E. Pyrite oxidation in carbonate-buffered solution: Experimental kinetics. *Geochim. Et Cosmochim. Acta* **1988**, *52*, 1077–1085. [CrossRef]

71. Nicholson, R.V.; Gillham, R.W.; Reardon, E.J. Pyrite oxidation in carbonate-buffered solution: Rate control by oxide coatings. *Geochim. Et Cosmochim. Acta* **1990**, *54*, 395–402. [CrossRef]

72. Chaudhri, A.R.; Mahavir, S. Clay Minerals as Climate Change Indicators—A Case Study. *Am. J. Clim. Change* **2012**, *1*, 231–239. [CrossRef]

73. Ruiz, R.M.; Blanco, C.G.; Pesquera, C.; González, F.; Benito, I.; López, J. Zeolitization of a bentonite and its application to the removal of ammonium ion from waste water. *Appl. Clay Sci.* **1997**, *12*, 73–83. [CrossRef]

74. Baccouche, A.; Srasra, E.; El Maaoui, M. Preparation of Na–P1 and sodalite octahydrate zeolites from interstratified illite–smectite. *Appl. Clay Sci.* **1998**, *13*, 255–273. [CrossRef]

75. Cañizares, P.; Duran, A.; Dorado, F.; Carmona, M. The role of sodium montmorillonite on bounded zeolite-type catalysts. *Appl. Clay Sci.* **2000**, *16*, 273–287. [CrossRef]

76. Gualtieri, A.F. Synthesis of sodium zeolites from a natural halloysite. *Phys. Chem. Miner.* **2001**, *28*, 719–728. [CrossRef]

77. Boukadir, D.; Bettahar, N.; Derriche, Z. Synthesis of zeolites 4A and HS from natural materials. *Ann. De Chim. Sci. Des. Mater.* **2002**, *27*, 1–13. [CrossRef]

78. Shawabkeh, R.; Al-Harahsheh, A.; Hami, M.; Khlaifat, A. Conversion of oil shale ash into zeolite for cadmium and lead removal from wastewater. *Fuel* **2004**, *83*, 981–985. [CrossRef]

79. Shawabkeh, R.; Al-Harahsheh, A.; Al-Otoom, A. Production of zeolite from Jordanian oil shale ash and application for zinc removal from wastewater. *Oil Shale* **2004**, *21*, 125–136.

80. Fernandes-Machado, N.R.C.; Miotto-Bigatão, D.M.M. Synthesis of Na–A and –X zeolites from oil shale ash. *Fuel* **2005**, *84*, 2289–2294. [CrossRef]

81. Fernandes-Machado, N.R.C.; Miotto-Bigatão, D.M.M. Use of zeolites synthesized from oil shale ash for arsenic removal from polluted wáter. *Química Nova* **2007**, *30*, 1108–1114. [CrossRef]

82. Abdmeziem-Hamoudi, K.; Siffert, B. Synthesis of molecular sieve zeolites from a smectite-type clay material. *Appl. Clay Sci.* **1989**, *4*, 1–9. [CrossRef]

83. Kovo, A.S.; Hernandez, O.; Holmes, S.M. Synthesis and characterization of zeolite Y and ZSM-5 from Nigerian Ahoko Kaolin using a novel, lower temperature, metakaolinization technique. *J. Mater. Chem.* **2009**, *19*, 6207–6212. [CrossRef]

84. Hamadi, A.; Nabih, K. Alkali Activation of Oil Shale Ash Based Ceramics. *E-J. Chem.* **2012**, *9*, 1373–1388. [CrossRef]

85. Ngoc, D.T.; Pham, T.H.; Nguyen, K.D.H. Synthesis, characterization and application of nanozeolite NaX from Vietnamese kaolin. *Adv. Nat. Sci. Nanosci. Nanotechnol.* **2013**, *4*, 1–12. [CrossRef]

86. Bao, W.W.; Zou, H.F.; Gan, S.C.; Xu, X.C.; Ji, G.J.; Zheng, K.Y. Adsorption of heavy metal ions from aqueous solutions by zeolite based on oil shale ash: Kinetic and equilibrium studies. *Chem. Res. Chin. Univ.* **2013**, *29*, 126–131. [CrossRef]

87. Zhou, Z.; Jin, G.; Liu, H.; Wu, J.; Mei, J. Crystallization mechanism of zeolite A from coal kaolin using a two-step method. *Appl. Clay Sci.* **2014**, *97–98*, 110–114. [CrossRef]

88. Tong, L.; Luo, H.; Zhang, L.; Zhan, H. Preparation of single phase Na–X zeolite from oil shale ash by melting hydrothermal method. *China's Refract.* **2014**, *23*, 12–17.

89. Doyle, A.M.; Alismaeel, Z.T.; Albayati, T.M.; Abbas, A.S. High purity FAU-type zeolite catalysts from shale rock for biodiesel production. *Fuel* **2017**, *199*, 394–402. [CrossRef]

90. Bai, S.-X.; Zhou, L.-M.; Chang, Z.-B.; Zhang, C.; Chu, M. Synthesis of Na–X zeolite from Longkou oil shale ash by alkaline fusion hydrothermal method. *Carbon Resour. Convers.* **2018**, *1*, 245–250. [CrossRef]

91. Akolekar, D.; Chaffee, A.; Howe, R.F. The transformation of kaolin to low-silica X zeolite. *Zeolites* **1997**, *19*, 359–365. [CrossRef]

92. Xu, M.; Cheng, M.; Tan, D.; Liu, X.; Bao, X. Growth of zeolite KSO1 on calcined kaolin microspheres. *J. Mater. Chem.* **1999**, *9*, 2965–2966. [CrossRef]

93. Eze, K.A.; Nwadiogbu, J.O.; Nwankwere, E.T. Effect of Acid Treatments on the Physicochemical Properties of Kaolin Clay. *Arch. Appl. Sci. Res.* **2012**, *4*, 792–794.

94. Murat, M.; Amokrane, A.; Bastide, J.P.; Montanaro, L. Synthesis of zeolites from thermally activated kaolinite. Some observations on nucleation and growth. *Clay Miner.* **1992**, *27*, 119–130. [CrossRef]

95. Chandrasekhar, S.; Pramada, P.N. Investigation on the Synthesis of Zeolite NaX from Kerala Kaolin. *J. Porous Mater.* **1999**, *6*, 283–297. [CrossRef]

96. Novembre, D.; Di Sabatino, B.; Gimeno, D.; Pace, C.; Sabatino, D. Synthesis and characterization of Na–X, Na–A and Na–P zeolites and hydroxysodalite from metakaolinite. *Clay Miner.* **2011**, *46*, 339–354. [CrossRef]

97. Sanhueza, V.; Kelm, U.; Cid, R. Synthesis of molecular sieves from Chilean kaolinites: Synthesis of NaA type zeolites. *J. Chem. Technol. Biotechnol.* **1999**, *74*, 358–363. [CrossRef]

98. Belviso, C.; Cavalcante, F.; Lettino, A.; Fiore, S. A and X-type zeolites synthesised from kaolinite at low temperatura. *Appl. Clay Sci.* **2013**, *80–81*, 162–168. [CrossRef]

99. Basaldella, E.I.; Kikot, A.; Tara, J.C. Effect of pellet pore size and synthesis conditions in the in situ synthesis of LSX zeolite. *Ind. Eng. Chem. Res.* **1995**, *34*, 2990–2996. [CrossRef]

100. Covarrubias, C.; García, R.; Arriagada, R.; Yánez, J.; Garland, M.T. Cr(III) exchange on zeolites obtained from kaolin and natural mordenite. *Microporous Mesoporous Mater.* **2006**, *88*, 220–231. [CrossRef]

101. Chorover, J.; Choi, S.; Amistadi, M.K.; Karthikeyan, K.G.; Crosson, G.; Mueller, K.T. Linking Cesium and Strontium Uptake to Kaolinite Weathering in Simulated Tank Waste Leachate. *Environ. Sci. Technol.* **2003**, *37*, 2200–2208. [CrossRef]

102. Buhl, J.C.; Löns, J. Synthesis and crystal structure of nitrate enclathrated sodalite $Na_8[AlSiO_4]_6(NO_3)_2$. *J. Alloy. Compd.* **1996**, *235*, 41–47. [CrossRef]

103. Healey, A.; Johnson, G.; Weller, M. The synthesis and characterization of JBW-type zeolites. *Microporous Mesoporous Mater.* **2000**, *37*, 153–163. [CrossRef]

104. Lin, D.-C.; Xu, X.-W.; Zuo, F.; Long, Y.-C. Crystallization of JBW, CAN, SOD and ABW type zeolite from transformation of metakaolin. *Microporous Mesoporous Mater.* **2004**, *70*, 63–70. [CrossRef]

105. Ríos, C.A.; Williams, C.D.; Castellanos, O.M. Synthesis and characterization of zeolites by alkaline activation of kaolinite and industrial by-products (fly ash and natural clinker). *Bistua* **2006**, *4*, 60–71.

106. Ríos, C.A.; Williams, C.D.; Maple, M. Synthesis of zeolites and zeotypes by hydrothermal transformation of kaolinite and metakaolinite. *Bistua* **2007**, *5*, 15–26.

107. Ríos, C.A.; Williams, C.D.; Castellanos, O.M. Synthesis of zeolite LTA from thermally treated kaolinite. *Rev. Fac. Ing.* **2010**, *53*, 30–41.

108. Ríos, C.A.; Williams, C.D. Hydrothermal transformation of kaolinite in the system K_2O-SiO_2-Al_2O_3-H_2O. *DYNA Univ. Nac. Colomb. Medellin* **2010**, *77*, 55–63.

109. Ríos, C.A.; Williams, C.D.; Roberts, C.L. Synthesis and characterisation of SOD-, CAN- and JBW-type structures by hydrothermal reaction of kaolinite at 200 °C. *DYNA Univ. Nac. Colomb. Medellin* **2011**, *78*, 38–47.